Research Article

Nano Research
2023, 16(2): 3312–3319

ISSN 1998-0124 CN 11-5974/O4
https://doi.org/10.1007/s12274-022-4937-7

# Bio-inspired superhydrophobic magnesium alloy surfaces with active anti-corrosion and self-healing properties

Qiang Li[1], Xudong Zhang[1], Shuang Ben[1], Zhihong Zhao[1], Yuzhen Ning[2] (✉), Kesong Liu[1] (✉), and Lei Jiang[1]

[1] *Key Laboratory of Bio-Inspired Smart Interfacial Science and Technology School of Chemistry, Beihang University, Beijing 100191, China*
[2] *School of Mechanical Engineering and Automation, Beihang University, Beijing 100191, China*



**Received:** 1 July 2022 / **Revised:** 8 August 2022 / **Accepted:** 18 August 2022

## ABSTRACT

Bio-inspired superhydrophobic magnesium (Mg) alloy surfaces are of increasing interest in corrosion protection due to superior barrier and shielding effects. However, superhydrophobic (SHB) anti-corrosion surfaces are susceptible to damage, which limit their extensive applications. To this end, a micro/nano structure-functional molecule SHB composite coating with self-healing and active anti-corrosion dual-function properties was designed on Mg alloys substrate. The dual-function SHB composite anti-corrosion coating based on lauric acid (La) intercalated and modified hydrotalcite (La-LDH) consisted of three-layer structure, namely La-LDH powder/polydimethylsiloxane (PDMS)/La-LDH film. The anti-corrosion performance of as-prepared coatings was investigated by potentiodynamic polarization and electrochemical impedance spectroscopy (EIS). The results indicate that the SHB coating shows excellent active corrosion resistance. Moreover, we also examined the self-healing and anti-corrosion properties of SHB coating upon physical damage and explained the healing mechanism. After heat treatment, the damaged SHB coating regain its surface microstructure and corrosion protection property. This work expands new insights for the wide application of Mg alloys and the research in the field of metal protection.

## KEYWORDS

magnesium alloys, anti-corrosion coating, superhydrophobic, self-healing, active anti-corrosion property

## 1 Introduction

Light metal materials are widely used in electronics, automobiles, aerospace, biomedicine devices and other fields attributed to their abundant resources and low density [1–3]. Magnesium (Mg) alloys are one of the most promising light metal materials due to its peculiar properties of excellent biocompatibility, high strength, good heat/electrical conductivity, and shock absorption [4, 5]. However, poor corrosion resistance of Mg alloys is a major obstacle limiting their more extensive applications [6, 7]. To solve the problem of poor corrosion resistance, a lot of anti-corrosion methods have been proposed to improve the anti-corrosion performances of Mg alloys [1, 4, 6]. Among these methods, constructing superhydrophobic (SHB) surfaces is one of the common and effective methods to protect Mg alloys [8–10]. Inspired by several plants and animals in nature, the artificial SHB coatings were constructed by the synergistic interaction of micro-nanostructure and low surface energy [6, 10, 11]. SHB surfaces can form a thin air layer between the liquid and the metal to reduce the contact area of corrosive liquid with the Mg alloys surface [12–15]. Traditionally, the corrosion protection properties of SHB anti-corrosion coatings are improved from two aspects. One is to exploit self-healing SHB anti-corrosion coatings. Damages of the coating surfaces are inevitable due to the physical and chemical attacks (scratches, mechanical impacts, and salt-spray fog) during use. SHB anti-corrosion coatings are more susceptible to damage. Once the SHB anti-corrosion coating is damaged, it will not be able to protect the metal surface, which is one of the most important reasons that hinder its widely application [16, 17]. The SHB coating with self-healing ability is capable of self-healing after being damaged, thus providing multiple protection for the metal substrate. While the other is to provide the active anti-corrosion function by the incorporation of corrosion inhibitors. The release of the corrosion inhibitors reduces the rate of the corrosion reaction, thus providing active anti-corrosion protection. The introduction of corrosion inhibitors into SHB anti-corrosion coatings can significantly improve the active corrosion resistance of the coatings, which is more conducive to the protection of metal substrates, especially light metals [18–21]. In this context, it is still need to exploit a SHB coating combining self-healing and active anti-corrosion functions.

Based on these, introducing smart polymers into SHB coatings will be a promising strategy to prepare self-healing SHB anti-corrosion coatings. A variety of smart organic polymers have been used for preparing self-healing coating [22], such as epoxy resin [23], polyurethane [24], polydimethylsiloxane (PDMS) [25], polyethyleneimine/polyacrylic acid [26], polycaprolactone [27] and so on. The special laminated structure of hydrotalcite (layered double hydroxide, LDH) ensures this material as an ideal nanoparticle for constructing SHB coatings. In addition, LDH in possession of unique inter-layer ion exchange character can intercalate corrosion inhibitive anions, thereby serving as a corrosion inhibitor reservoir. Correspondingly, the LDH release inhibitor ions through ion-exchange process capture aggressive $Cl^-$ to protect the metal substrate, which makes them have active anti-

Address correspondence to Kesong Liu, liuks@buaa.edu.cn; Yuzhen Ning, ningyuzhen@buaa.edu.cn

corrosion function [28–30]. Inorganic compounds are commonly employed as the corrosion inhibitor on LDH, for instance, tungstate [29], vanadate [31], and molybdate [32]. But these inorganic corrosion inhibitors are hidden danger of the human and environment [33]. While because of the special functional groups, the organic compounds may have better inhibition effect than the inorganic [34]. Given this, more and more organic corrosion inhibitors with green and non-hazardous properties have been exploited, for instance, lauric acid (La) [35], phytic acid [36], and methionine [37].

Herein, we innovatively developed a method for fabricating the micro/nano structure-functional molecule SHB composite anti-corrosion coating that combines active anti-corrosion and self-healing dual-function properties. The dual-function SHB composite anti-corrosion coatings consisted of a top layer of LDH powders, an intermediate layer of PDMS, and a bottom layer of LDH film. LDH powders and LDH film were modified and intercalated with La (La-LDH). The modification and intercalation of LDH powder with La endows the coating top layer with hydrophobic and active anti-corrosion characters, which can be served as a nano-reservoir for corrosion inhibitors and also provides a crucial micro-nano structure for creating roughness of SHB surface. The intermediate layer PDMS act as a binder to anchor the La-LDH powders tightly on the substrate. Moreover, the C–H chains provided by PDMS could migrate to the surface by a simple heat treatment to heal damage once the coatings surface is damaged [25, 38]. Corrosion inhibitive ions could be released on demand by the bottom La-LDH film. The bottom layer of La-LDH film and top layer of LDH powders becomes the nano-reservoir of La, which realizes multiple protection of the Mg alloys substrate. This further strengthened the active anti-corrosion performances of coatings. Afterward, the self-healing and active anti-corrosion performances of as-prepared coatings were investigated by potentiodynamic polarization and electrochemical impedance spectroscopy (EIS). The results demonstrate that the as-prepared SHB coatings possess superior self-healing ability and anti-corrosion performance. Noteworthily, after simple heat treatment, the scratches of SHB composite anti-corrosion coatings can be fully healed and the barrier performance can be almost completely recovered. Therefore, this work will hopefully extend the applications of Mg alloys and other metal materials under harsh wetting conditions, and provide a guidance for the exploration of SHB-based multifunctional anti-corrosion coatings.

## 2 Experimental

### 2.1 Materials

AZ31B Mg alloys (Al 3.1%, Zn 0.93%, Mn 0.26%, Fe 0.0016%, Si 0.011%, Cu 0.0012%, Ni 0.00069%, and balanced Mg) was purchased from Xinbiao Co. (Hebei, China), with a size of 20 mm × 30 mm × 1 mm. $Mg(NO_3)_2{\cdot}6H_2O$ (99%), $Al(NO_3)_3{\cdot}9H_2O$ (99%), hexyl hydride (97%), NaCl (99.5%), urea (99.5%), and sodium laurate (98%) were analytical grade. PDMS (SYLGARD 184) and curing agent were provided by Dow Corning Corporation.

### 2.2 Sample preparation

The La-LDH powders were synthesized by a coprecipitation process. $Mg(NO_3)_2{\cdot}6H_2O$ (0.02 mol), $Al(NO_3)_3{\cdot}9H_2O$ (0.01 mol) and urea (0.28 mol) were dissolved in 200 mL deionized water and maintained at 90 °C for 24 h under stirring. After the reaction, the 0.1 mol sodium laurate was added to the above mixture solution and further reacted at 90 °C for 10 h. The La-LDH powder was obtained by centrifugation, washed with water and ethanol and then dried at 50 °C for 12 h. The AZ31B Mg alloys were polished with 600, 1,000, 1,500, and 2,000 SiC abrasive papers, then ultrasonically cleaned in absolute ethyl alcohol and dried in air. $Mg(NO_3)_2{\cdot}6H_2O$ (0.01 mmol), $Al(NO_3)_3{\cdot}9H_2O$ (0.005 mmol), and urea (0.015 mmol) were dissolved in 100 mL deionized water. Then, the mixed solution was transferred to 100 mL Teflon-lined autoclaves with AZ31B Mg alloy sheets placed vertically inside and heated to 120 °C for 12 h. Replace mixed solution by 0.2 M sodium laurate solution to prepare La-LDH films. The SHB composite coatings were prepared by a simple spray approach. 1 g PDMS and curing agent in a weight ratio of 10 : 1 was dissolved in hexyl hydride (10 ml) and stirred at 30 °C for 4 h. Then, the obtained solution was sprayed onto La-LDH film with a 0.6 MPa compressed air (the spray distance was 10 cm, the spraying time was 10 s) and pre-cured at 70 °C for 12 min. Subsequently, La-LDH powder were sprayed onto PDMS surface. Finally, the SHB composite coatings were cured at 80 °C for 4 h.

### 2.3 Characterization and instruments

The surface microstructures of the coatings were examined using a scanning electron microscopy (SEM, Quanta 250 FEG). An energy-dispersive X-ray spectrum (EDS) detector was used to analyzed the chemical composition. Contact angle (CA) measurement was conducted using an OCA20 machine (Data-Physics, Germany). The crystal structure of the coatings was tested by X-ray diffraction (XRD, LabX XRD-6000, Cu K$\alpha$, $\lambda$ = 0.15406 nm). Fourier transform infrared spectroscopy (FTIR) spectrum of coatings surface was analyzed by Excalibur HE 3100 (Fourier, USA).

The corrosion-inhibiting performance of La was tested by the ion chromatograph (IC, Thermo Scientific Dionex ICS-5000). The AZ31B, AZ31B with LDH coating, and AZ31B with La-LDH coating were immersed in the NaCl solution (3.5 wt.%) and then the $Mg^{2+}$ concentration in the filtrate after immersed for different times were tested by IC. The anion-exchange performance of SHB coating was analyzed by FTIR spectrum. The SHB coating was immersed in 3.5 wt.% NaCl solution for 24 h and then the filtrate was analyzed by FTIR spectrum.

EIS, open circuit potential (OCP), and potentiodynamic polarization curves were performed on electrochemical workstation (CHI660E, Chenhua) with a three-electrode system. The as-prepared sample, platinum electrode, and Ag/AgCl electrode were used as the working electrode, the counter electrode, and the reference electrode, respectively. All the electrodes were immersed in the NaCl solution (3.5 wt.%).

The self-healing ability of the SHB coating surface was characterized by alternation of scalpel cutting and heat treatment. The as-prepared SHB coating surface was cut with a scalpel. The scratched sample was subjected to a heat treatment at 105 °C for 2 h to heal the damages. SEM and EIS were performed on the scratched sample and healed sample. The linear abrasion test was carried out using 1,000 grit SiC sandpaper as an abrasion surface. The SHB coating surface with a weight of 100 g above it was put face-down to SiC sandpaper and moved 10 cm.

## 3 Results and discussion

### 3.1 Preparation and characterization of the coatings

The fabrication process of the micro/nano structure-functional molecule SHB composite coating is illustrated in Fig. 1. Firstly, LDH powder was fabricated by a coprecipitation process in the mixed solution containing $Mg(NO_3)_2{\cdot}6H_2O$, $Al(NO_3)_3{\cdot}9H_2O$ and urea. Afterward, the sodium laurate was added into the coprecipitation solution to modify the LDH and inserted into the

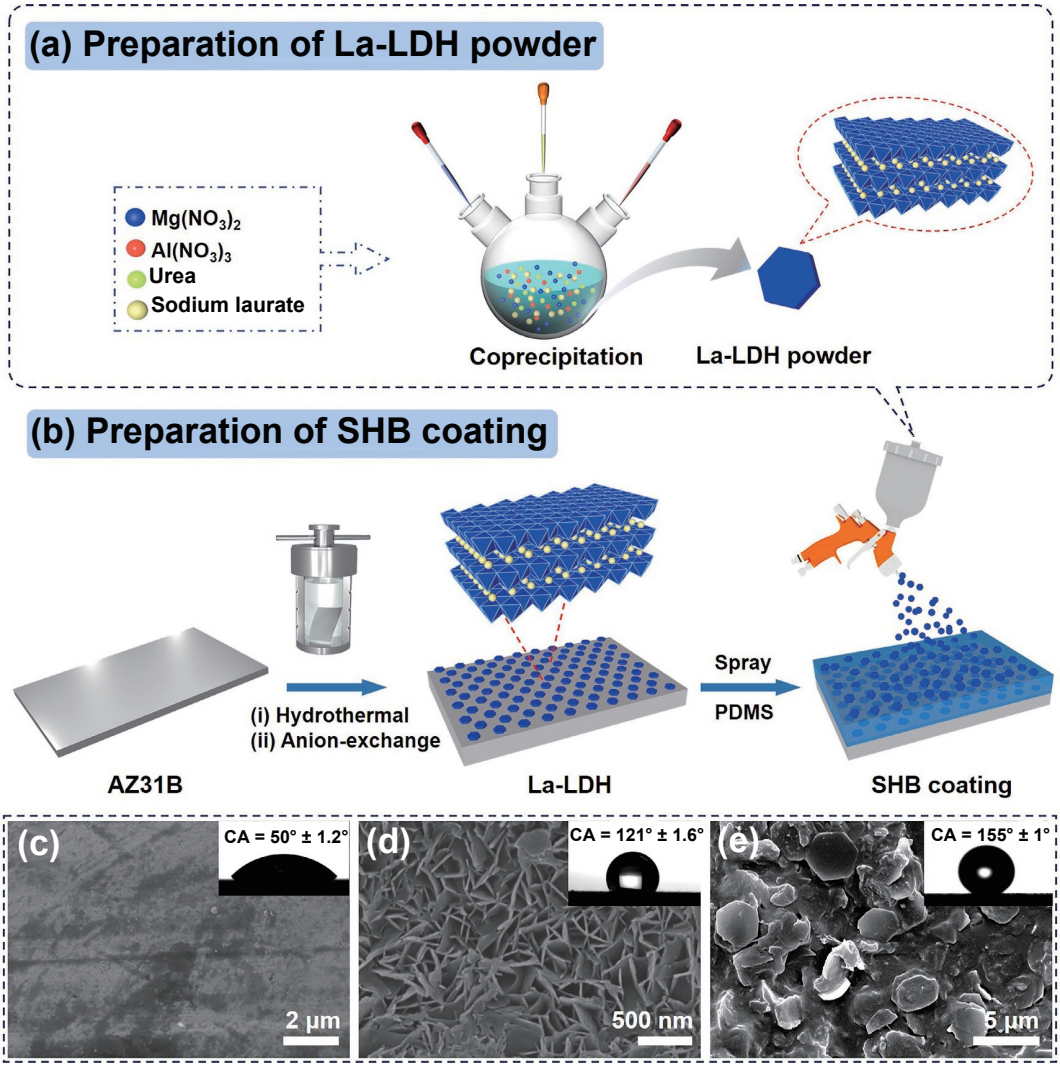


**Figure 1** Schematic preparation procedure and SEM images of the micro/nano structure-functional molecule SHB composite coatings. (a) The synthesis diagram of La-LDH powders by coprecipitation process. (b) The preparation process of the dual-function SHB composite anti-corrosion coatings. ((c)–(e)) SEM images and corresponding contact angle photographs of the coating surface. (c) The untreated Mg alloy surface possesses a relatively smooth surface and present a hydrophilic character. (d) The La-LDH conversion film at the bottom layer of the coating is fused by hydrothermal reaction and anion-exchange. The La-LDH coating surface demonstrates a hydrophobic condition. (e) The microstructure image of SHB coating surface at the top layer of the coating. After La-LDH powders spraying, the SHB coating possesses a micro/nano multiscale surface structure and reveals a superhydrophobic status.

lamellar structure of LDH to obtain La-LDH powder (Fig. 1(a)). As shown in Fig. 1(b), we prepared a LDH coating *in situ* on the Mg alloys substrate by the hydrothermal reaction, and then modified and intercalated the LDH coating by anion-exchange to obtained a La-LDH coating. Thereafter, a layer of PDMS was deposited on the La-LDH film and then the as-prepared La-LDH powder was sprayed, and subsequently the dual-function SHB composite anti-corrosion coating was obtained. As revealed by the Figs. 1(c)–1(e), the morphology and wettability of the coating surfaces experienced obvious change during the fabrication process. At the optimum growth concentration, the LDH nanoplates evenly cover the whole alloys surface (Fig. S1 in the Electronic Supplementary Material (ESM)). However, due to the hydrophilicity of LDH, the surface of Mg alloys covered with LDH coating is still hydrophilic. This hydrophilicity makes corrosive species prone to accumulate in LDH coating, eventually initiating corrosion. The hydrophilicity character of LDH coating reversed after the anion-exchange process, which is due to the modification of La with low surface energy, increasing the water contact angle to 121° (Fig. 1(d)). The hydrophobicity character of compacted La-LDH powder (CA ≈ 137°, Fig. S2(a) in the ESM) is better than La-LDH coating, owing to the more fully modification and intercalation of the powder during the coprecipitation process. After PDMS and La-LDH powder spraying, the La-LDH powder not only escalated the surface micro/nanoscale hierarchical structures but also further lowered the surface energy of coating (Fig. 1(e)). The synergistic effect of suitable micro/nanoscale hierarchical structures and low surface energy endows the coating with SHB property, and the CA of final coating is 155° (Fig. 1(e)). The top layer of La-LDH powders can reduce the contact with the corrosive liquid (3.5 wt.% NaCl solution droplet contact angle is 154°, Fig. S2(b) in the ESM) and avoid the waste of corrosion inhibitor. Moreover, the SHB coating still maintained superhydrophobicity even after standing for 15 days (CA ≈ 152°, Fig. S2(c) in the ESM). After abrasion test, the CA of the SHB coating is 148° (Fig. S2(d) in the ESM), indicating the better abrasive resistance property of the SHB coating.

To confirm the structure and composition of the SHB composite coating surface, we analyzed it by some advanced tests and evaluated its corrosion-inhibiting performance. The chemical composition of SHB coating surface was analyzed by EDS (Figs. 2(a) and 2(b)). The Au element comes from the gold spraying before sample testing. It can be seen that the main chemical components of the SBH coating are Mg, Al, Si, C, and O elements.

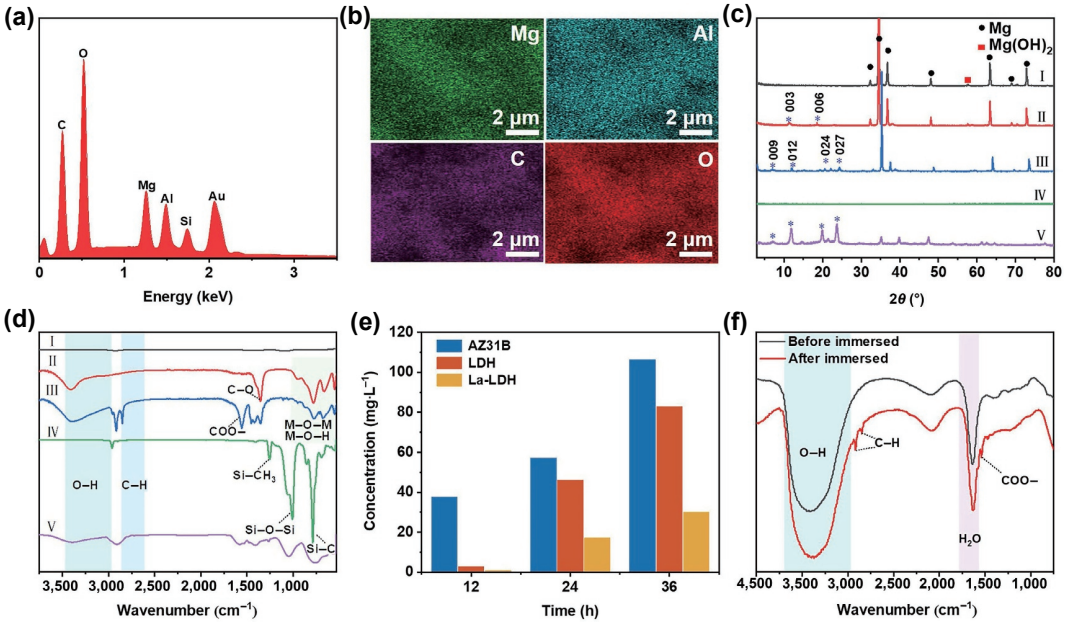


**Figure 2** Characterization of coatings. ((a) and (b)) Surface elements analysis: EDS spectra of SHB coating. (c) XRD patterns and (d) FTIR spectra of (I) Mg alloy substrate, (II) LDH coating, (III) La-LDH coating, (IV) PDMS/La-LDH coating, and (V) SHB coating. The typical characteristic peaks and absorption bands of La anion embedded into the LDH interlayer appeared in spectrum. (e) Corrosion-inhibiting performance test: the $Mg^{2+}$ concentration in the filtrate of the AZ31B, AZ31B with LDH coating, and AZ31B with La-LDH coating after immersed in 3.5 wt.% NaCl solution for different time. (f) Anion-exchange performance test: the FTIR spectra of La-LDH coating before and after exposure in 3.5 wt.% NaCl solution for 24 h.

The content of Mg and Al are mainly derived from the sprayed La-LDH powders. Si, C, H, and O elements are mainly derived from PDMS and La modified on the surface of La-LDH powders. Figure 2(c) exhibits the XRD results of the as-prepared specimens. The spectrum of LDH coating (Fig. 2(c), II) shows typical (003) and (006) layered characteristic peaks of LDH, which is in good accordance with the reported literature [28, 39, 40]. In spectrum of La-LDH and SHB coating (Fig. 2(c), III and V), the peaks at 7.1° and 11.9° correspond to the (009) and (012) planes, respectively, indicating that La anions have been successfully intercalated into LDH gallery. This fact is identical with the previous results of La intercalated LDH materials [39]. Nevertheless, these characteristic peaks vanished in the XRD pattern of PDMS/La-LDH coating (Fig. 2(c), IV), which is mainly attributed to the coverage of the amorphous PDMS layer. Figure 2(d) displays the FTIR spectra of all samples. The broad absorption band in the 3,650–3,200 $cm^{-1}$ is attributed to O–H stretching vibration in the LDHs laminate. The absorption band in the 950–570 $cm^{-1}$ is associated with M–O–H bending vibrations and M–O–M skeletal stretching (M means metal element). For the La-LDH coating (Fig. 2(d), III), new absorption peaks at 2,849 and 2,918 $cm^{-1}$ are assigned to the tensile vibration of the alkyl C–H group, and the peak at 1,557 $cm^{-1}$ is characteristic of the symmetrical and asymmetric vibration of the COO– group. These results indicate that the La anions were successfully embedded into the LDH interlayer. In the spectrum of PDMS/La-LDH coating (Fig. 2(d), IV), the spectra at 1,255, 1,007, and 786 $cm^{-1}$ are assigned to the PDMS component (Si–$CH_3$, Si–O–Si, and Si–C). The decreased intensity of the broad absorption band at 3,750–3,060 $cm^{-1}$ as well as the La characteristic peak which is mainly attributed to the shielding effect of the PDMS. The peak at 1,380 $cm^{-1}$ can be assigned to the carbonate groups which can be ascribed to the interfere of atmospheric $CO_2$ (Fig. 2(d), II) [29]. The change in the absorption band intensity of the SHB coating (Fig. 2(c), V) can be ascribed to the spraying of La-LDH powders. The results verify that SHB coating surface has the expected three-layer structure, namely La-LDH powder/PDMS/La-LDH film. We further evaluated the corrosion inhibition performance by measuring the $Mg^{2+}$ concentration in NaCl solution. The AZ31B, AZ31B with LDH coating, and AZ31B with La-LDH coating were immersed in a 3.5 wt.% NaCl solution for different time, and then the concentration of $Mg^{2+}$ in the filtrate were measured (Fig. 2(e)). It can be seen that the concentration of the $Mg^{2+}$ increases with the immersed time. By contrast, the corrosion rate of La-LDH coating is slower, which is due to the LDH film intercalated with La anions can significantly protect the Mg substrate. In order to further study the release mechanism of the La corrosion inhibitive ions, the NaCl solution (3.5 wt.%) immersed of La-LDH coating for 24 h was characterized by the FTIR spectroscopic technique (Fig. 2(f)). It is easy to find that the absorption peaks of C–H group and COO– group appeared in the NaCl solution after immersing La-LDH coating after 24 h, which means that the intercalated La ions underwent anion-exchange process with $Cl^-$ and were released. Based on the above results, the La anions were successfully intercalated into the LDH interlayer and can capture $Cl^-$ in the corrosion media to protect the substrate.

### 3.2 Anti-corrosion performance

We investigated the anti-corrosion performance by measuring the potentiodynamic polarization curves. The potentiodynamic polarization curves (tested in 3.5 wt.% NaCl aqueous solution) of AZ31B substrate and four different kinds of coatings are demonstrated in Fig. 3(a), and the corresponding corrosion current density ($I_{corr}$) and corrosion potential ($E_{corr}$) are listed in Table 1. It shows that the $E_{corr}$ of AZ31B bare substrate was the most negative among all samples. After hydrothermal treatment of Mg alloys substrate, the obtained LDH coating presented a more positive $E_{corr}$, however, the value of $I_{corr}$ is close to that of the substrate. Ordinarily, lower $I_{corr}$ (or higher $E_{corr}$) means slower interface reaction and better anti-corrosion performance [26, 35, 41]. This implies that the LDH coating with hydrophilic property cannot improve the corrosion resistance significantly. The La-LDH sample presents a distinctly lower $I_{corr}$ in comparison with AZ31B substrate and LDH coating, suggesting that the modification and intercalation of La can improve the corrosion resistance obviously. The $I_{corr}$ of La-LDH and PDMS/La-LDH

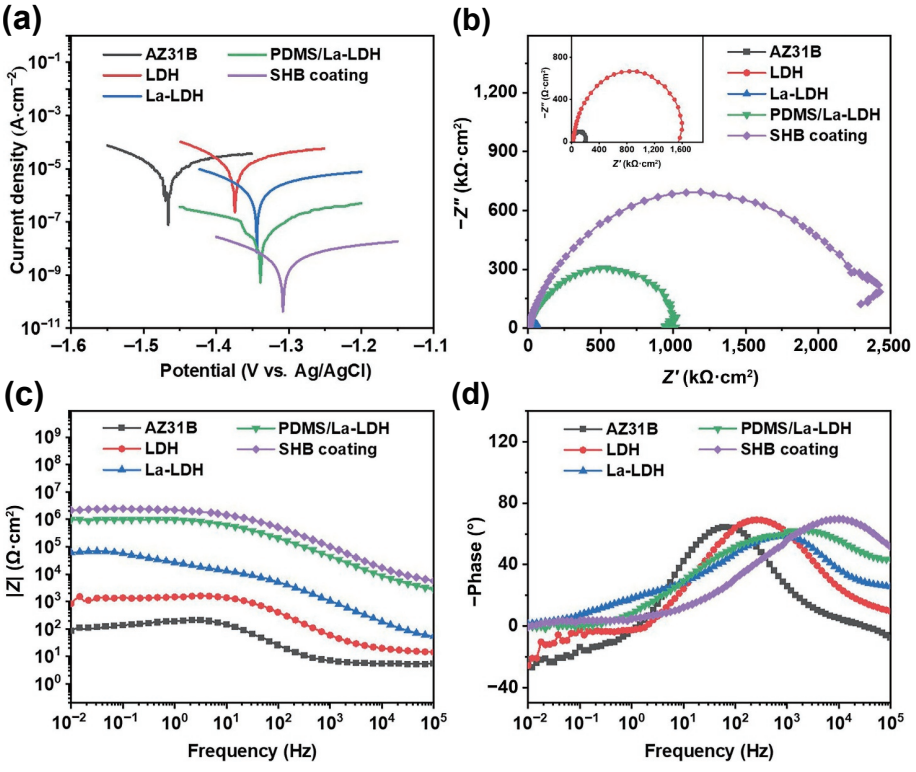


**Figure 3** Electrochemical test in 3.5 wt.% NaCl solution at room temperature. (a) Potentiodynamic polarization curves: the SHB coating showed more positive $E_{corr}$ and lower $I_{corr}$. (b) Nyquist plots: the SHB coating has largest capacitive arc. The module plots of impedance (c) and the phase plots of impedance (d).

**Table 1** Fitting results of the potentiodynamic curves in 3.5 wt.% NaCl solution.

| Sample | $E_{corr}$ (V) | $I_{corr}$ (A·cm$^{-2}$) |
|---|---|---|
| AZ31B | −1.465 | $1.834 \times 10^{-5}$ |
| LDH | −1.375 | $2.450 \times 10^{-5}$ |
| La-LDH | −1.344 | $5.717 \times 10^{-6}$ |
| PDMS/La-LDH | −1.339 | $1.065 \times 10^{-7}$ |
| SHB coating | −1.307 | $6.447 \times 10^{-9}$ |

decreases to $5.717 \times 10^{-6}$ and $1.065 \times 10^{-7}$ A·cm$^{-2}$, respectively, indicating that the PDMS coating can provide a well-protective barrier. Compared with the $I_{corr}$ of the PDMS/La-LDH, the $I_{corr}$ of the SHB coating ($6.447 \times 10^{-9}$ A·cm$^{-2}$) is reduced by two orders of magnitude. This is because of the formation of air trapped and the release of corrosion inhibitive anions on the surface of coating, which can reduce and inhibit the infiltration of corrosive ions. The results of polarization measurements illustrate that the SHB anti-corrosion coating can effectively enhance the corrosion resistance of Mg alloys substrate. OCP can further estimate the corrosion resistance of the coatings. Compared with the other coatings, the SHB coating has the highest potential value, indicating the best corrosion resistance (Fig. S3(a) in the ESM).

To further demonstrate the anti-corrosion performances of different kinds of coatings in NaCl solution, we also measured the coatings by EIS method (Fig. 3(b) and Fig. S3(b) in the ESM). The equivalent circuits of different coatings are presented in Fig. S3 in the ESM, respectively. There are apparent differences in the axial radius of the Nyquist plot between each sample. The axial radius of the four coatings is much larger than the Mg alloys substrate, which reveals that these coatings have excellent chemical impermeability and inertness, making it hard for the aggressive anions ($Cl^-$) to reach the substrate surface. Due to the presence of trapped air and corrosion-inhibiting anions in the SHB coating, the axial radius of the SHB coating is much larger than other coatings, indicating that the SHB coating has the best anti-corrosion performance. It is well accepted that larger impedance modulus at the low-frequency domain is an indication of better corrosion resistance [26, 35, 41]. As shown in Fig. 3(c), the impedance modulus of La-LDH is clearly higher than that of LDH at the low-frequency domain, suggesting that the modification and intercalation of La can reduce and inhibit the intrusion of aggressive medium (Fig. 3(c)). Notably, the SHB coating shows the largest value of impedance modulus (0.01 Hz), which is four orders of magnitude higher than that of Mg alloys substrate, indicating that the SHB coating has a very excellent anti-corrosion performance. From the relationship between phase angle and frequency , it can be seen that all the samples manifest a wide peak at medium or high frequency domain, revealing that the corrosion reaction on coating surfaces was controlled by the charge transfer process [42]. Furthermore, the SHB coating exhibits the highest phase angle at high frequencies (Fig. 3(d)), suggesting that it is difficult for the aggressive anions ($Cl^-$) to permeate into inner position of the coating. The combination of the SHB and corrosion-inhibiting function brings about a synergic shielding effect, which greatly enhances the anti-corrosion function of the SHB coating.

### 3.3 Self-healing ability of the SHB coating

We also examined the self-healing property and anti-corrosion performance of SHB coating upon physical damage. The intact SHB coating (Figs. 4(a), 4(d), and 4(g)) was scratched with a scalpel, leading to severe damage of surface microstructure (Fig. 4(b)). SEM images show that a cut with a width around 35 μm in the damaged area (Figs. 4(e) and 4(h)). In the view of optical picture, the scratches almost fully healed after heat treatment, and the coating obtain recovery just as prior to damage (Fig. 4(c)). SEM images indicate the cut with micron level disappeared miraculously, and the damage area of the SHB coating was re-combined (Figs. 4(f) and 4(i)). The healed micro/nano multiscale structure at the damaged area is similar to that before scratched

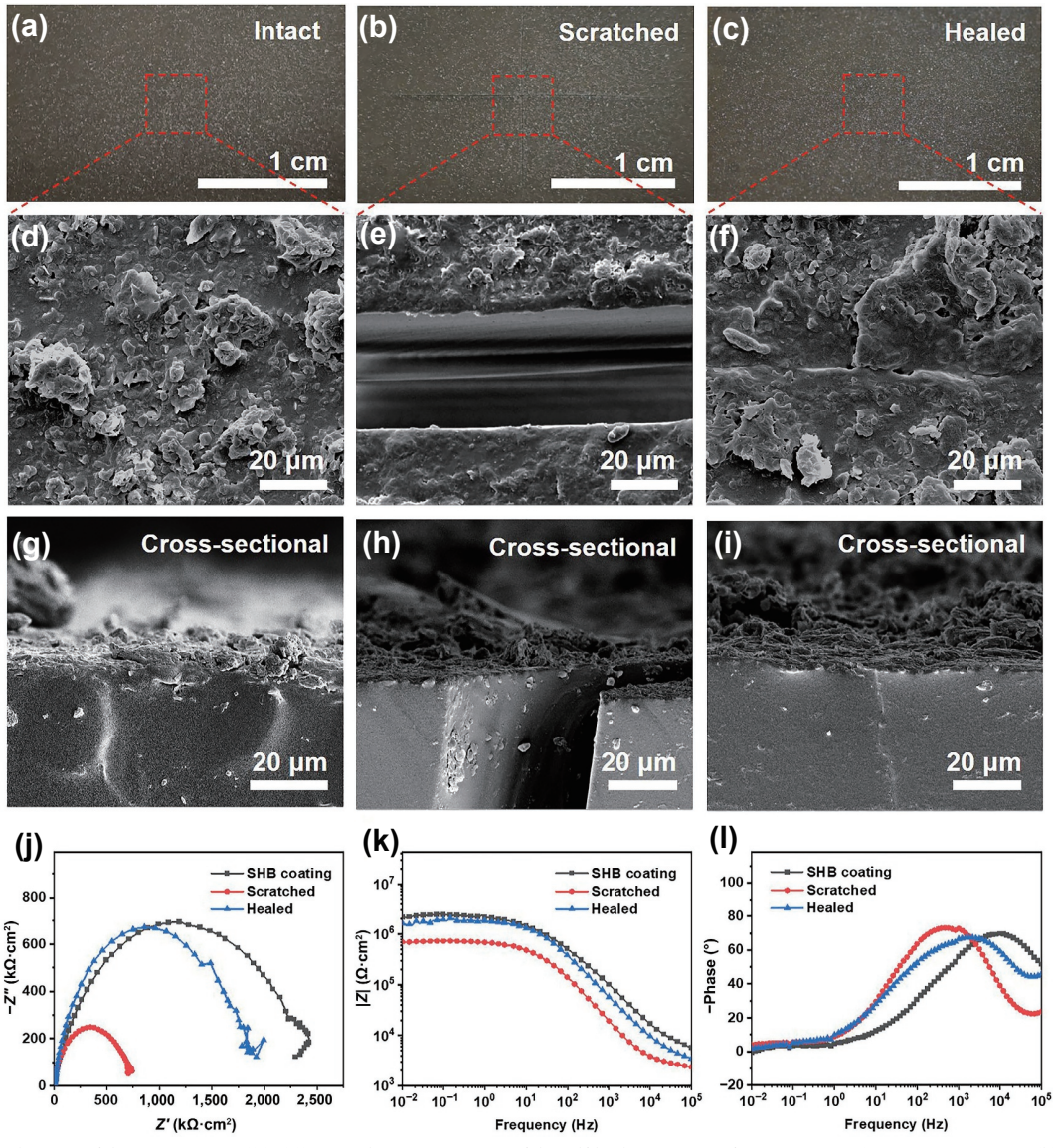


**Figure 4** Self-healing test of the SHB coating. ((a)–(c)) Optical top-view images of the self-healing process of SHB coating. (a) Intact SHB coating, (b) scratched SHB coating in the center using a scalpel, and (c) healed SHB coating after heat treatment (105 °C). ((d)–(f)) Top-view SEM images and ((g)–(i)) corresponding cross-sectional SEM photos of SHB coating. After heat treatment, the scratch on the SHB coating surface healed and without obvious scar. ((j)–(l)) The electrochemical test of SHB coating before and after healed in a 3.5 wt.% NaCl solution. (j) Nyquist plots, (k) the module plots of impedance, and (l) phase angle versus frequency plots. The healed coating exhibited great corrosion protection property.

(Fig. 4(f)). The EDS spectra (Fig. S4 in the ESM) indicated that the chemical composition of the healed SHB coating hardly changed after heat treatment. Moreover, the healed SHB coating can still maintain superhydrophobicity after heat treatment (CA ≈ 153°, Fig. S4(c) in the ESM). Due to the damage of the SHB coating surface, the corrosive ions could easily invade into the interface between the coating and the Mg alloys substrate. Therefore, the capacitive arc diameter of the scratched coating is decreased by about one order of magnitude, and both the impedance modulus at low frequencies and the phase angle at high frequencies are clear lower than the intact coating. However, the barrier properties on the damaged area were almost completely recovered after healed (Fig. 4(j)), and the aggressive medium hardly penetrate to the inner position of the coating. Eventually, phase angle and impedance modulus analysis results indicate that the healed coating repossess the great anti-corrosion property, which can rival to the undamaged coating (Figs. 4(k) and 4(l)). Hence, the as-prepared SHB coating has superior self-healing ability and anti-corrosion performance.

### 3.4 Mechanism discussion

To better apply the dual-function SHB composite anti-corrosion coating, we deeply studied the mechanism of self-healing and active anti-corrosion. The LDH intercalated with inhibitors have been extensively researched and proven to endow the LDH based coating with active corrosion protection property, which is ascribed to the release of corrosion inhibitor [28, 29, 35, 39]. The release behavior is caused by the anion-exchange process with $Cl^-$ and laurate ion (Fig. 5(a)). By trapping the corrosive $Cl^-$ and releasing inhibitive La ion, the SHB coating could significantly reduce the corrosion rate. Therefore, the La ions were detected in the NaCl solution (3.5 wt.%) immersed of SHB coating for 24 h (Fig. 2(e)). Once the surface of SHB coating is scratched (Fig. 5(b)), the interior of coating will be exposed, resulting in an increase of surface free energy of the coating surface. During heat treatment, the functional molecules of PDMS on subsurface become mobile. The C–H chains (healing agent and low surface energy components) provided by PDMS migrated to the top of the surface and then accumulated at the uppermost layer, eventually recombined [43]. In this way, the scratched SHB coating perfectly healed (Fig. 5(c)). Therefore, after heat treatment, the SHB coating regained its surface microstructure and anti-

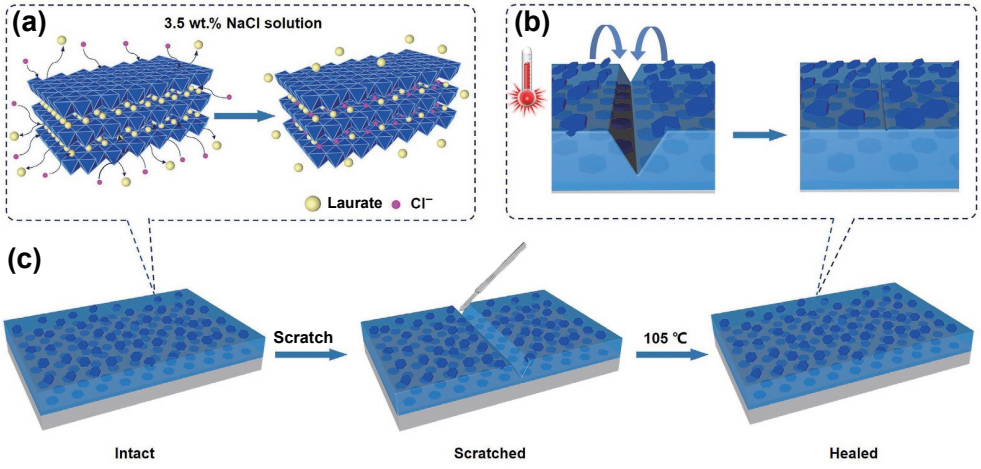


**Figure 5** Schematic illustration of self-healing and active anti-corrosion mechanism of dual-function SHB anti-corrosion coating. (a) By ani-on-exchange process the corrosive $Cl^-$ were trapped and inhibitive La ions were released. (b) During heat treatment, the C–H chains migrated to the damage area driven by the surface free energy minimization, and then recombined. (c) Scratching and self-healing process of SHB coating.

corrosion performance. This phenomenon is mainly attributed to the minimization of surface energy on the coating surface, which is a spontaneous process during heat treatment (105 °C) [44].

The excellent corrosion protection property of as-prepared dual-function SHB composite anti-corrosion coating is due to the synergistic effect of the following: i) the La-LDH powder top layer act as physical barriers and corrosion inhibitor nano-reservoirs. The uppermost layer can inhibit the direct contact between corrosive medium and metal substrate, and release La inhibitor to protect the substrate when the coating is damaged. Moreover, the air-film of SHB coating prevents the direct contact of corrosion solution and avoids unnecessary waste of corrosion inhibitor. ii) The presence of the PDMS intermediate layer endows the as-prepared SHB coating self-healing ability. At 105 °C, the functional C–H chain of PDMS will migrate to the damaged area via thermal motion and recombine, which induce the good self-healing ability. iii) The La-LDH bottom layer can further enhance the corrosion resistance of Mg alloys substrate and release corrosion inhibitor laurate ion on demand. Consequently, the dual-function SHB coating enables the Mg alloys substrates possess both self-healing and active anti-corrosion abilities.

## 4 Conclusions

In conclusion, we designed a micro/nano structure-functional molecule SHB composite coating integrating self-healing and active anti-corrosion dual-functions for AZ31B substrate. The static contact angle of SHB composite coating is 155°. The SHB coating obviously reduce the $I_{corr}$ ($6.447 \times 10^{-9}$ A·cm$^{-2}$) and has a superior corrosion protection property. Moreover, we studied the corrosion resistance and self-healing ability of as-prepared SHB coating. The La-LDH endows the coating with hydrophobic and active anti-corrosion properties and can act as a nano-reservoir for corrosion inhibitors. By trapping the corrosive $Cl^-$ and releasing inhibitive La ion, the SHB coating could significantly reduce the corrosion rate. Moreover, the air-film of SHB coating can reduce the contact with the corrosive liquid and avoid the waste of corrosion inhibitor. After heat treatment, the scratched coating surface can heal its microstructure. The self-healing mechanism is because of the migration of functional C–H chain with low surface energy provided by PDMS, driven by the minimize of the surface free energy. Additionally, the fabrication method is totally green, and avoiding the use of hazardous or deleterious corrosion inhibitor. This dual-function SHB composite anti-corrosion coating provides a new idea to for the development of new multifunctional anti-corrosion coatings.

## Acknowledgements

This work was supported by the Fundamental Research Fund (No. 2020-JCJQ-JJ-008), the National Natural Science Foundation of China (No. 21871020), and the Postdoctoral Research Foundation of China (Nos. 2021TQ0023, 2020M680296, 2022T150035 and 2022TQ0022).

**Electronic Supplementary Material:** Supplementary material (including further details of the SEM images, contact angle photographs, EDS images, and electrochemical measurement, etc.) is available in the online version of this article at https://doi.org/10.1007/s12274-022-4937-7.

## References

[1] Luo, Q.; Guo, Y. L.; Liu, B.; Feng, Y. J.; Zhang, J. Y.; Li, Q.; Chou, K. Thermodynamics and kinetics of phase transformation in rare earth-magnesium alloys: A critical review. *J. Mater. Sci. Technol.* **2020**, *44*, 171–190.

[2] Song, M. S.; Zeng, R. C.; Ding, Y. F.; Li, R. W.; Easton, M.; Cole, I.; Birbilis, N.; Chen, X. B. Recent advances in biodegradation controls over Mg alloys for bone fracture management: A review. *J. Mater. Sci. Technol.* **2019**, *35*, 535–544.

[3] Zheng, Q. Y.; Li, J.; Yuan, W.; Liu, X. M.; Tan, L.; Zheng, Y. F.; Yeung, K. W. K.; Wu, S. L. Metal–organic frameworks incorporated polycaprolactone film for enhanced corrosion resistance and biocompatibility of Mg alloy. *ACS Sustainable Chem. Eng.* **2019**, *7*, 18114–18124.

[4] Wang, Y. C.; Liu, B. Y.; Zhao, X. A.; Zhang, X. H.; Miao, Y. C.; Yang, N.; Yang, B.; Zhang, L. Q.; Kuang, W. J.; Li, J. et al. Turning a native or corroded Mg alloy surface into an anti-corrosion coating in excited $CO_2$. *Nat. Commun.* **2018**, *9*, 4058.

[5] Xu, T. C.; Yang, Y.; Peng, X. D.; Song, J. F.; Pan, F. S. Overview of advancement and development trend on magnesium alloy. *J. Magnes. Alloys* **2019**, *7*, 536–544.

[6] Zhang, J. L.; Gu, C. D.; Tu, J. P. Robust slippery coating with superior corrosion resistance and anti-icing performance for AZ31B Mg alloy protection. *ACS Appl. Mater. Interfaces* **2017**, *9*, 11247–11257.

[7] Liu, H. G.; Cao, F. Y.; Song, G. L.; Zheng, D. J.; Shi, Z. M.; Dargusch, M. S.; Atrens, A. Review of the atmospheric corrosion of magnesium alloys. *J. Mater. Sci. Technol.* **2019**, *35*, 2003–2016.

[8] Li, Y. L.; Luong, D. X.; Zhang, J. B.; Tarkunde, Y. R.; Kittrell, C.; Sargunaraj, F.; Ji, Y.; Arnusch, C. J.; Tour, J. M. Laser-induced graphene in controlled atmospheres: From superhydrophilic to superhydrophobic surfaces. *Adv. Mater.* **2017**, *29*, 1700496.

[9] Zaffora, A.; Di Franco, F.; Virtù, D.; Carfì Pavia, F.; Ghersi, G.;

Virtanen, S.; Santamaria, M. Tuning of the Mg Alloy AZ31 anodizing process for biodegradable implants. *ACS Appl. Mater. Interfaces* **2021**, *13*, 12866–12876.

[10] Zhu, Y. J.; Sun, F. L.; Qian, H. J.; Wang, H. Y.; Mu, L. W.; Zhu, J. H. A biomimetic spherical cactus superhydrophobic coating with durable and multiple anti-corrosion effects. *Chem. Eng. J.* **2018**, *338*, 670–679.

[11] Zhao, S. Y.; Yang, X. T.; Xu, Y. Y.; Weng, Z. Z.; Liao, L.; Wang, X. L. A sprayable superhydrophobic dental protectant with photo-responsive anti-bacterial, acid-resistant, and anti-fouling functions. *Nano Res.* **2022**, *15*, 5245–5255.

[12] Liu, Y. J.; Guo, Y. J.; Zhang, X. Q.; Gao, G. Q.; Shi, C. Q.; Huang, G. Z.; Li, P. L.; Kang, Q.; Huang, X. Y.; Wu, G. N. Self-cleaning of superhydrophobic nanostructured surfaces at low humidity enhanced by vertical electric field. *Nano Res.* **2022**, *15*, 4732–4738.

[13] Zhang, X.; Wang, Q.; Zou, R. P.; Song, B.; Yan, C. Z.; Shi, Y. S.; Su, B. 3D-printed superhydrophobic and magnetic device that can self-powered sense a tiny droplet impact. *Engineering*, in press, DOI: https://doi.org/10.1016/j.eng.2022.04.009.

[14] Ma, Z.; Wang, Q.; Wu, Z. H.; Chen, D. Z.; Yan, C. Z.; Shi, Y. S.; Dickey, M. D.; Su, B. A superconducting-material-based maglev generator used for outer-space. *Adv. Mater.* **2022**, *32*, 2203814.

[15] Ma, Z.; Ai, J. W.; Shi, Y. S.; Wang, K.; Su, B. A superhydrophobic droplet-based magnetoelectric hybrid system to generate electricity and collect water simultaneously. *Adv. Mater.* **2020**, *32*, 2006839.

[16] Lu, Y.; Sathasivam, S.; Song, J. L.; Crick, C. R.; Carmalt, C. J.; Parkin, I. P. Robust self-cleaning surfaces that function when exposed to either air or oil. *Science* **2015**, *347*, 1132–1135.

[17] Zhou, H. M.; Chen, R. R.; Liu, Q.; Liu, J. Y.; Yu, J.; Wang, C.; Zhang, M. L.; Liu, P. L.; Wang, J. Fabrication of ZnO/epoxy resin superhydrophobic coating on AZ31 magnesium alloy. *Chem. Eng. J.* **2019**, *368*, 261–272.

[18] Hollamby, M. J.; Fix, D.; Dönch, I.; Borisova, D.; Möhwald, H.; Shchukin, D. Hybrid polyester coating incorporating functionalized mesoporous carriers for the holistic protection of steel surfaces. *Adv. Mater.* **2011**, *23*, 1361–1365.

[19] Haase, M. F.; Grigoriev, D. O.; Möhwald, H.; Shchukin, D. G. Development of nanoparticle stabilized polymer nanocontainers with high content of the encapsulated active agent and their application in water-borne anticorrosive coatings. *Adv. Mater.* **2012**, *24*, 2429–2435.

[20] Shchukin, D.; Möhwald, H. A coat of many functions: Smart coatings are designed to be sensitive to various external and internal stimuli, thereby enhancing the surface functionality of materials. *Science* **2013**, *341*, 1458–1459.

[21] Son, G. C.; Hwang, D. K.; Jang, J.; Chee, S. S.; Cho, K.; Myoung, J. M.; Ham, M. H. Solution-processed highly adhesive graphene coatings for corrosion inhibition of metals. *Nano Res.* **2019**, *12*, 19–23.

[22] Yang, K.; Duan, Y. X.; Liu, G. C.; Ma, G. Y.; Fu, H.; Chen, X. Y.; Wang, M. X.; Zhu, G. Q.; Yang, W.; Shen, Y. D. Smart ZnS@C filler for super-anticorrosive self-healing zinc-rich epoxy coating. *Nano Res.* **2022**, *15*, 4756–4764.

[23] Zhao, X.; Wei, J. F.; Li, B. C.; Li, S. B.; Tian, N.; Jing, L. Y.; Zhang, J. P. A self-healing superamphiphobic coating for efficient corrosion protection of magnesium alloy. *J. Colloid Interf. Sci.* **2020**, *575*, 140–149.

[24] Li, Y. B.; Li, B. C.; Zhao, X.; Tian, N.; Zhang, J. P. Totally waterborne, nonfluorinated, mechanically robust, and self-healing superhydrophobic coatings for actual anti-icing. *ACS Appl. Mater. Interfaces* **2018**, *10*, 39391–39399.

[25] Wang, Y. K.; Liu, Y. P.; Li, J.; Chen, L. W.; Huang, S. L.; Tian, X. L. Fast self-healing superhydrophobic surfaces enabled by biomimetic wax regeneration. *Chem. Eng. J.* **2020**, *390*, 124311.

[26] Fan, F.; Zhou, C. Y.; Wang, X.; Szpunar, J. Layer-by-layer assembly of a self-healing anticorrosion coating on magnesium alloys. *ACS Appl. Mater. Interfaces* **2015**, *7*, 27271–27278.

[27] Huang, L.; Li, J.; Yuan, W.; Liu, X. M.; Li, Z. Y.; Zheng, Y. F.; Liang, Y. Q.; Zhu, S. L.; Cui, Z. D.; Yang, X. J. et al. Near-infrared light controlled fast self-healing protective coating on magnesium alloy. *Corros. Sci.* **2020**, *163*, 108257.

[28] Cao, Y. H.; Zheng, D. J.; Li, X. L.; Lin, J. Y.; Wang, C.; Dong, S. G.; Lin, C. J. Enhanced corrosion resistance of superhydrophobic layered double hydroxide films with long-term stability on Al substrate. *ACS Appl. Mater. Interfaces* **2018**, *10*, 15150–15162.

[29] Ding, C. D.; Tai, Y.; Wang, D.; Tan, L. H.; Fu, J. J. Superhydrophobic composite coating with active corrosion resistance for AZ31B magnesium alloy protection. *Chem. Eng. J.* **2019**, *357*, 518–532.

[30] Wang, X.; Jing, C.; Chen, Y. X.; Wang, X. S.; Zhao, G.; Zhang, X.; Wu, L.; Liu, X. Y.; Dong, B. Q.; Zhang, Y. X. Active corrosion protection of super-hydrophobic corrosion inhibitor intercalated Mg–Al layered double hydroxide coating on AZ31 magnesium alloy. *J. Magnes. Alloys* **2020**, *8*, 291–300.

[31] Tedim, J.; Zheludkevich, M. L.; Bastos, A. C.; Salak, A. N.; Lisenkov, A. D.; Ferreira, M. G. S. Influence of preparation conditions of Layered Double Hydroxide conversion films on corrosion protection. *Electrochim. Acta* **2014**, *117*, 164–171.

[32] Zeng, R. C.; Liu, Z. G.; Zhang, F.; Li, S. Q.; Cui, H. Z.; Han, E. H. Corrosion of molybdate intercalated hydrotalcite coating on AZ31 Mg alloy. *J. Mater. Chem. A* **2014**, *2*, 13049–13057.

[33] Skorb, E. V.; Skirtach, A. G.; Sviridov, D. V.; Shchukin, D. G.; Möhwald, H. Laser-controllable coatings for corrosion protection. *ACS Nano* **2009**, *3*, 1753–1760.

[34] Bereket, G.; Yurt, A. The inhibition effect of amino acids and hydroxy carboxylic acids on pitting corrosion of aluminum alloy 7075. *Corros. Sci.* **2001**, *43*, 1179–1195.

[35] Song, Y. H.; Tang, Y.; Fang, L.; Wu, F.; Zeng, X. G.; Hu, J.; Zhang, S. F.; Jiang, B.; Luo, H. J. Enhancement of corrosion resistance of AZ31 Mg alloys by one-step *in situ* synthesis of ZnAl-LDH films intercalated with organic anions (ASP, La). *J. Magnes. Alloys* **2021**, *9*, 658–667.

[36] Chen, J.; Song, Y. W.; Shan, D. Y.; Han, E. H. Modifications of the hydrotalcite film on AZ31 Mg alloy by phytic acid: The effects on morphology, composition and corrosion resistance. *Corros. Sci.* **2013**, *74*, 130–138.

[37] Yan, D. S.; Wang, Y. L.; Liu, J. L.; Song, D. L.; Zhang, T.; Liu, J. Y.; He, F.; Zhang, M.; Wang, J. Self-healing system adapted to different pH environments for active corrosion protection of magnesium alloy. *J. Alloys Compd.* **2020**, *824*, 153918.

[38] Tu, K.; Wang, X. Q.; Kong, L. Z.; Guan, H. Facile preparation of mechanically durable, self-healing and multifunctional superhydrophobic surfaces on solid wood. *Mater. Des.* **2018**, *140*, 30–36.

[39] Zhang, F. Z.; Zhao, L. L.; Chen, H. Y.; Xu, S. L.; Evans, D. G.; Duan, X. Corrosion resistance of superhydrophobic layered double hydroxide films on aluminum. *Angew. Chem. Int. Ed.* **2008**, *47*, 2466–2469.

[40] Yarger, M. S.; Steinmiller, E. M. P.; Choi, K. S. Electrochemical synthesis of Zn–Al layered double hydroxide (LDH) films. *Inorg. Chem.* **2008**, *47*, 5859–5865.

[41] Afshari, M.; Mohammadloo, H. E.; Sarabi, A. A.; Roshan, S. Modification of hydroxyapatite-based coating in the presence of polyvinylalcohol (PVA) for implant application: Corrosion, structure and surface study. *Corros. Sci.* **2021**, *192*, 109859.

[42] Chen, H. Y.; Wang, F. F.; Fan, H. Z.; Hong, R. Y.; Li, W. H. Construction of MOF-based superhydrophobic composite coating with excellent abrasion resistance and durability for self-cleaning, corrosion resistance, anti-icing, and loading-increasing research. *Chem. Eng. J.* **2021**, *408*, 127343.

[43] Long, M. Y.; Peng, S.; Deng, W. S.; Miao, X. R.; Wen, N.; Zhou, Q. N.; Yang, X. J.; Deng, W. L. A robust superhydrophobic PDMS@ZnSn$(OH)_6$ coating with under-oil self-cleaning and flame retardancy. *J. Mater. Chem. A* **2017**, *5*, 22761–22771.

[44] Li, B. C.; Zhang, J. P. Durable and self-healing superamphiphobic coatings repellent even to hot liquids. *Chem. Commun.* **2016**, *52*, 2744–2747.